Cell-autonomous expression of the acid hydrolase galactocerebrosidase

Christina R. Mikulka[a], Joshua T. Dearborn[a], Bruno A. Benitez[b], Amy Strickland[c], Lin Liu[a,1], Jeffrey Milbrandt[c], and Mark S. Sands[a,c,2]

[a]Department of Medicine, Washington University School of Medicine, St. Louis, MO 63110; [b]Department of Psychiatry, Washington University School of Medicine, St. Louis, MO 63110; and [c]Department of Genetics, Washington University School of Medicine, St. Louis, MO 63110

Edited by William S. Sly, Saint Louis University School of Medicine, St. Louis, MO, and approved March 11, 2020 (received for review October 9, 2019)

Lysosomal storage diseases (LSDs) are typically caused by a deficiency in a soluble acid hydrolase and are characterized by the accumulation of undegraded substrates in the lysosome. Determining the role of specific cell types in the pathogenesis of LSDs is a major challenge due to the secretion and subsequent uptake of lysosomal hydrolases by adjacent cells, often referred to as "cross-correction." Here we create and validate a conditional mouse model for cell-autonomous expression of galactocerebrosidase (GALC), the lysosomal enzyme deficient in Krabbe disease. We show that lysosomal membrane-tethered GALC (GALCLAMP1) retains enzyme activity, is able to cleave galactosylsphingosine, and is unable to cross-correct. Ubiquitous expression of GALCLAMP1 fully rescues the phenotype of the GALC-deficient mouse (Twitcher), and widespread deletion of GALCLAMP1 recapitulates the Twitcher phenotype. We demonstrate the utility of this model by deleting GALCLAMP1 specifically in myelinating Schwann cells in order to characterize the peripheral neuropathy seen in Krabbe disease.

lysosomal storage disease | Krabbe disease | mouse model

Lysosomal storage disorders (LSDs) are a large class of metabolic diseases. With more than 50 distinct diseases and an incidence of ∼1:5,000 live births, LSDs are among the most prevalent inherited pediatric disorders (1, 2). LSDs are typically caused by a deficiency in a soluble acid hydrolase and are characterized by the accumulation of undegraded substrates in the lysosome (3). Many current therapies for LSDs, including bone marrow transplantation, recombinant enzyme replacement therapy, and gene therapy, rely on the naturally occurring secretion of lysosomal enzymes and receptor-mediated uptake by nearby cells, commonly referred to as "cross-correction" (4). However, cross-correction prevents the cell-autonomous expression or deletion of lysosomal enzymes, and as such represents a major hurdle when determining the role of specific cell types in the pathogenesis of various LSDs.

Globoid cell leukodystrophy, or Krabbe disease (5), is an autosomal-recessive, invariably fatal neurological disorder caused by a deficiency of the ubiquitously expressed, soluble lysosomal enzyme galactocerebrosidase (GALC; ref. 6). GALC is responsible for the catabolism of certain galactosylated lipids, including the toxic compound galactosylsphingosine (psychosine; ref. 7). Due to its rapid accumulation in myelinating cells, psychosine kills oligodendrocytes and myelinating Schwann cells, leading to a demyelinating phenotype that affects both the central (CNS) and peripheral (PNS) nervous systems (8–10). It is unclear what roles central and peripheral nervous system pathologies play in the progression of Krabbe disease.

The murine model of Krabbe disease, the Twitcher ($GALC^{-/-}$) mouse, is a spontaneously arising null mutant (11). The Twitcher phenotype is characterized by psychosine accumulation in various tissues (12), accumulation of globoid cells in the CNS (13), weight loss (11), hind limb atrophy (11), and tremor (11). Due to cross-correction, cell-specific expression of soluble native GALC will not produce a cell-autonomous response. Thus, although this model is useful for preclinical testing, it has lower utility for investigating disease pathogenesis. Therefore, we have created a chimeric form of GALC (GALCLAMP1), where the enzyme is tethered to the lysosomal membrane via the transmembrane domain of lysosome-associated membrane protein-1 (LAMP1), such that enzymatically active GALC remains in the lumen of the lysosome. This effectively eliminates cross-correction of adjacent cells. Ubiquitous expression of GALCLAMP1 completely rescues the phenotype of the Twitcher mouse. Widespread deletion of GALCLAMP1 recapitulates the Twitcher phenotype. We demonstrate the utility of this model by knocking out GALCLAMP1 specifically in myelinating Schwann cells, thereby clarifying the role of the PNS pathology in Krabbe disease. This conditional model is not only an important tool for the cell-specific study of Krabbe pathology, it also serves as a proof-of-concept approach that can be adapted for the study of many lysosomal enzyme deficiencies.

Results

The transmembrane region and cytosolic tail of LAMP1 was genetically linked to the C terminus of the codon-optimized murine GALC cDNA via a six-glycine linker (Fig. 1*A*). The configuration of GALCLAMP1 is such that enzymatically active GALC is localized in the lumen of the lysosome. Enzyme activity, cross-correction, and substrate cleavage were all tested in vitro using a lentiviral vector expressing GALCLAMP1 from

Significance

Lysosomal storage disorders (LSDs) are one of the most prevalent inherited pediatric conditions. Although some LSDs were described over a century ago, we understand little about how specific cells contribute to pathogenesis. Most LSDs are caused by a lysosomal enzyme deficiency. Lysosomal enzymes can be secreted from one cell and correct neighboring cells (cross-correction). Cross-correction prevents cell-limited expression or deletion of lysosomal enzymes, making it impossible to determine the role of specific cells in LSDs. Here we describe a method to eliminate cross-correction while maintaining enzymatic function. We used this method to determine the role of specific cells (myelin-producing) in Krabbe disease. This same method could be used to determine the role of specific cells in most other LSDs.

Author contributions: C.R.M. and M.S.S. designed research; C.R.M., J.T.D., B.A.B., A.S., L.L., and M.S.S. performed research; C.R.M. and J.M. contributed new reagents/analytic tools; C.R.M., J.T.D., B.A.B., A.S., and M.S.S. analyzed data; and C.R.M. and M.S.S. wrote the paper.

The authors declare no competing interest.

This article is a PNAS Direct Submission.

[1]Present address: M6P Therapeutics, St. Louis, MO 63108.

[2]To whom correspondence may be addressed. Email: mssands@wustl.edu.

This article contains supporting information online at https://www.pnas.org/lookup/suppl/doi:10.1073/pnas.1917675117/-/DCSupplemental.

First published April 6, 2020.

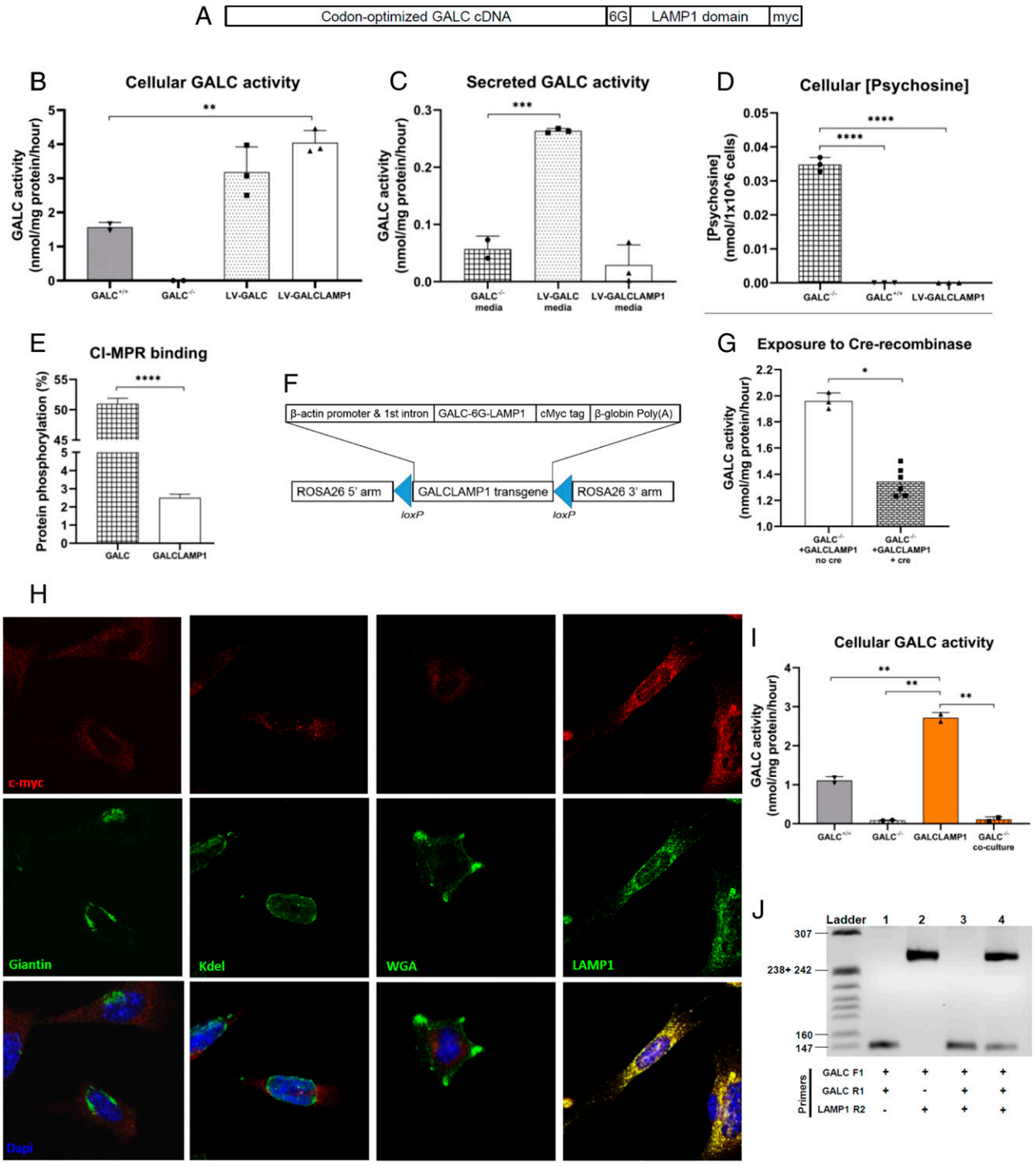

Fig. 1. Creation of GALCLAMP1 construct and in vitro testing. (*A*) GALCLAMP1 construct was created by linking codon-optimized GALC cDNA with the transmembrane region of LAMP1 via a six-glycine linker. A c-Myc tag was added at the C terminus. (*B*) GALC$^{-/-}$ cells transduced with LV-GALCLAMP1 have significantly higher GALC activity than WT (GALC$^{+/+}$). (*C*) Media from cells transduced with soluble GALC (LV-GALC media) has significantly higher GALC activity than media from either nontransduced Twitcher cells (GALC$^{-/-}$ media) or cells transduced with LV-GALCLAMP1. (*D*) GALC$^{-/-}$ fibroblasts transduced with LV-GALCLAMP1 have significantly lower psychosine levels than nontransduced GALC$^{-/-}$ cells and were not significantly different from those measured in GALC$^{+/+}$ cells. (*E*) Mannose-6-phosphorylation is significantly greater in soluble GALC compared to GALCLAMP1. (*F*) The GALCLAMP1 transgene was cloned downstream from the promoter and first intron of the chicken β-actin gene, followed by a rabbit β-globin polyadenylation signal. The transgene is flanked by LoxP sites and ROSA26 5′ and 3′ targeting arms. (*G*) Exposure to Cre-recombinase significantly reduces GALC activity in GALCLAMP1-expressing cells. (*H*) GALCLAMP1 (c-myc, red) did not colocalize with the Golgi complex (Giantin), endoplasmic reticulum (Kdel), or plasma membrane (WGA, green). Significant colocalization was only seen in the lysosome (LAMP1). DAPI (blue) staining identified the nucleus. (*I*) GALC-deficient cells cocultured with GALCLAMP1^{+} cells (GALC$^{-/-}$ coculture) have levels of GALC activity that are comparable to GALC$^{-/-}$ cells. (*J*) Analysis of the mRNA harvested from GALCLAMP1^{+} cells (lane 4) shows the presence of the GALCLAMP1 transcript at 266 bp. Control lanes containing cDNA from GALCLAMP1^{+} cells were analyzed with primers for GALC (lane 1; 146 bp) and GALCLAMP1 (lane 2; 266 bp). Analysis of the mRNA harvested from GALC$^{-/-}$ cells transduced with LV-GALC (lane 3) only show the presence of GALC transcript (*$P < 0.05$, **$P < 0.01$, ***$P < 0.001$, ****$P < 0.0001$).

the PGK promoter. GALC-deficient fibroblasts transduced with GALCLAMP1 have significantly higher levels of enzyme activity than $GALC^{+/+}$ cells (Fig. 1*B*). Enzyme activity in the media from the GALCLAMP1 transduced cells is equivalent to media from nontransduced GALC-deficient cells (Fig. 1*C*), indicating that GALCLAMP1 is not secreted into the media. GALC-deficient fibroblasts transduced with GALCLAMP1 have no detectable psychosine, indicating that GALCLAMP1 cleaves this toxic metabolite (Fig. 1*D*). To determine the phosphorylation status of GALCLAMP1, Expi293 cells were transfected with either a GALC- or GALCLAMP1-containing plasmid. By performing cation-independent (CI) MPR affinity chromatography (14), we determined the mannose phosphorylation of GALCLAMP1 to be at background level (Fig. 1*E*).

To create a conditional mouse model, the GALCLAMP1 transgene was subcloned downstream of the β-actin promoter to ensure ubiquitous expression. The expression cassette was flanked by LoxP sites to allow for Cre-recombinase–mediated excision of GALCLAMP1 (Fig. 1*F*). Targeting arms were used to ensure faithful insertion into a benign region of the genome between exons 1 and 2 of the ROSA26 locus. To determine if the ROSA-targeting construct was Cre-responsive, we stably transfected GALC-deficient fibroblasts with the ROSA26-targeting GALCLAMP1 plasmid. After transducing the selected GALCLAMP1-expressing cells with a Cre-expressing lentivirus, we saw a significant reduction in GALC activity, indicating that the transgene was excised (Fig. 1*G*).

GALCLAMP1 was integrated directly onto the C57BL/6 background using TALEN-directed insertion. Faithful integration into the ROSA26 locus was confirmed by PCR. Founder mice were bred onto the Twitcher colony to create a mouse that ubiquitously expresses GALCLAMP1 but not native soluble GALC [$ROSA^{Tg(GALCLAMP1)/+}$, $GALC^{-/-}$; henceforth referred to as $GALCLAMP1^{+}$]. A $GALCLAMP1^{+}$ dermal fibroblast cell line was isolated and used for ex vivo localization of GALCLAMP1. As expected, GALCLAMP1 (c-myc) localizes to the lysosome (LAMP1; Fig. 1*H*). In contrast, GALCLAMP1 did not colocalize with markers for the endoplasmic reticulum (Kdel), trans-Golgi network (giantin), or plasma membrane (WGA; Fig. 1*H*). When cocultured with GALC-deficient cells, $GALCLAMP1^{+}$ cells are unable to cross-correct, indicating that GALCLAMP1 is not secreted (Fig. 1*I*). Analysis of mRNA harvested from cells shows the presence of the GALCLAMP1 transcript (Fig. 1*J*).

A tissue survey from $GALCLAMP1^{+}$ mice shows high levels of GALC activity in all tissues at postnatal day (PND) 35 (Fig. 2*A*). Psychosine levels are undetectable in $GALCLAMP1^{+}$ tissues (Fig. 2*B*), indicating GALCLAMP1 can cleave this toxic substrate in vivo despite being tethered to the lysosomal membrane. Importantly, galactosylceramide levels in the brain at PND 35 are not different in $GALCLAMP1^{+}$ animals compared to $GALC^{+/+}$ (Fig. 2*C*), and similar results were seen at 1 y (*SI Appendix*, Fig. S1). GALC activity in serum of $GALCLAMP1^{+}$ animals following GALC immunoprecipitation shows very low levels of activity, no different from in $GALC^{-/-}$ animals, indicating that GALCLAMP1 is not being cleaved and released in a soluble form (Fig. 2*D*).

Histologically, $GALCLAMP1^{+}$ mice are indistinguishable from $GALC^{+/+}$ animals. Brains were stained using Luxol fast blue (LFB) and periodic acid–Schiff (PAS). The intensity of LFB staining and myelin organization in the $GALCLAMP1^{+}$ animals are similar to $GALC^{+/+}$, with no detectable globoid cells in the white matter (Fig. 2*F*). Sciatic nerves of these animals have heavily myelinated and densely packed axons that are indistinguishable from $GALC^{+/+}$ animals. The mean G-ratio of axons in the sciatic nerve of $GALCLAMP1^{+}$ mice is not significantly different from $GALC^{+/+}$ when measured at PND 35 (Fig. 2*E*). Myelin debris and infiltrating macrophages observed in the $GALC^{-/-}$ mice are not detected in the $GALCLAMP1^{+}$ mice (Fig. 2*F*). Mean G-ratio in the sciatic nerve of $GALC^{-/-}$ mice is significantly less at 6 wk compared to $GALC^{+/+}$ (*SI Appendix*, Fig. S2). Brains from PND 35 $GALCLAMP1^{+}$ mice stained for inflammatory markers CD68 and GFAP (*SI Appendix*, Fig. S3) are indistinguishable from $GALC^{+/+}$. Thin sections of spleen of 6-mo-old $GALCLAMP1^{+}$ mice show normal physiologic structures, and are similar to age-matched $GALC^{+/+}$mice (*SI Appendix*, Fig. S4).

When evaluated for a variety of behavioral abnormalities, $GALCLAMP1^{+}$ animals are indistinguishable from age-matched $GALC^{+/+}$ animals. With respect to motor function, $GALCLAMP1^{+}$ mice have the maximum latency of 60 s when tested on constant-speed rotarod and wire hang through 1 y of age (Fig. 3 *A* and *B*). The stride length and hind limb base of support (BOS) of these animals is also not significantly different from $GALC^{+/+}$ (Fig. 3 *C* and *D*). Resting tremor frequency of $GALC^{-/-}$ mice is very high. In contrast, resting tremor frequency of $GALC^{+/+}$ and $GALCLAMP1^{+}$ animals are significantly lower than $GALC^{-/-}$ and are not significantly different from each other (Fig. 3*E*). To determine if expression of GALCLAMP1 is toxic, we generated a mouse expressing both GALCLAMP1 and endogenous levels of soluble GALC [$ROSA^{Tg(GALCLAMP1)/+}$, $GALC^{+/+}$; henceforth referred to as $GALCLAMP1^{+}GALC^{+/+}$]. There was no decrease in life span (*SI Appendix*, Fig. S5) and no change in BOS or tremor compared to $GALC^{+/+}$ or $GALCLAMP1^{+}$ animals (Fig. 3 *D* and *E*).

To further validate the model, we ubiquitously deleted the GALCLAMP1 transgene using the CMV^{cre} mouse line [$ROSA^{Tg(GALCLAMP1)/+}$, CMV^{flox}, $GALC^{-/-}$; henceforth referred to as CMV^{flox}]. The CMV^{flox} animals have a median lifespan of 41 d, which is not significantly different from Twitcher mice (Fig. 4*A*). Very low levels of GALC activity were detected in brain, spinal cord, and sciatic nerve at PND 35 (Fig. 4*B*), and high psychosine levels were detected in these same tissues (Fig. 4*C*). The performance of CMV^{flox} mice on rotarod and wire hang also mirrors that of Twitcher mice (Fig. 4 *D* and *E*). In addition, the resting tremor frequency is not significantly different from Twitcher mice (Fig. 4*F*), and the stride length and hind limb BOS are identical (*SI Appendix*, Fig. S6). LFB/PAS staining shows disorganized myelin similar to Twitcher mice, with a large number of globoid cells in the CNS white matter (Fig. 4*G*). Finally, sciatic nerves of CMV^{flox} mice have poorly myelinated axons with a G-ratio and inflammatory infiltrates similar to Twitcher mice (Fig. 4 *G* and *H*).

The contribution of PNS pathology to the Twitcher phenotype was determined using the Myelin protein $zero^{cre}$ (MPZ^{cre}) mouse line (15), which removes GALCLAMP1 from myelinating Schwann cells in the peripheral nerves [$ROSA^{Tg(GALCLAMP1)/+}$, MPZ^{flox}, $GALC^{-/-}$; henceforth referred to as MPZ^{flox}]. GALC activity in the sciatic nerves of MPZ^{flox} mice is not significantly lower than $GALCLAMP1^{+}$ mice at either PND 35 or 1 y (Fig. 5*A*), partially due to the presence of GALCLAMP1 in the axons in the sciatic nerve. Although psychosine levels are significantly elevated at PND 35 in the sciatic nerves of MPZ^{flox} mice, this increase is not observed at 1 y of age (Fig. 5*B*). MPZ^{flox} mice survive to at least 1 y of age and can perform a rotarod test at $GALC^{+/+}$ levels through 1 y (Fig. 5*C*). Resting tremor frequency of MPZ^{flox} animals does not differ significantly from $GALCLAMP1^{+}$ animals at any age up to 1 y (Fig. 5*D*). Hind limb BOS significantly increases in MPZ^{flox} mice at PND 35; however, this difference is not maintained out to 1 y of age (Fig. 5*E*). LFB/PAS staining shows normal levels and organization of myelin in the brain, in particular the cerebellum, of MPZ^{flox} mice, with no evidence of globoid cells at either PND 35 or 1 y (Fig. 5*F*). Staining for $CD68^{+}$ inflammatory cells in the brain of MPZ^{flox} mice is similar to that seen in the $GALCLAMP1^{+}$ animals at PND 35 (*SI Appendix*, Fig. S7).

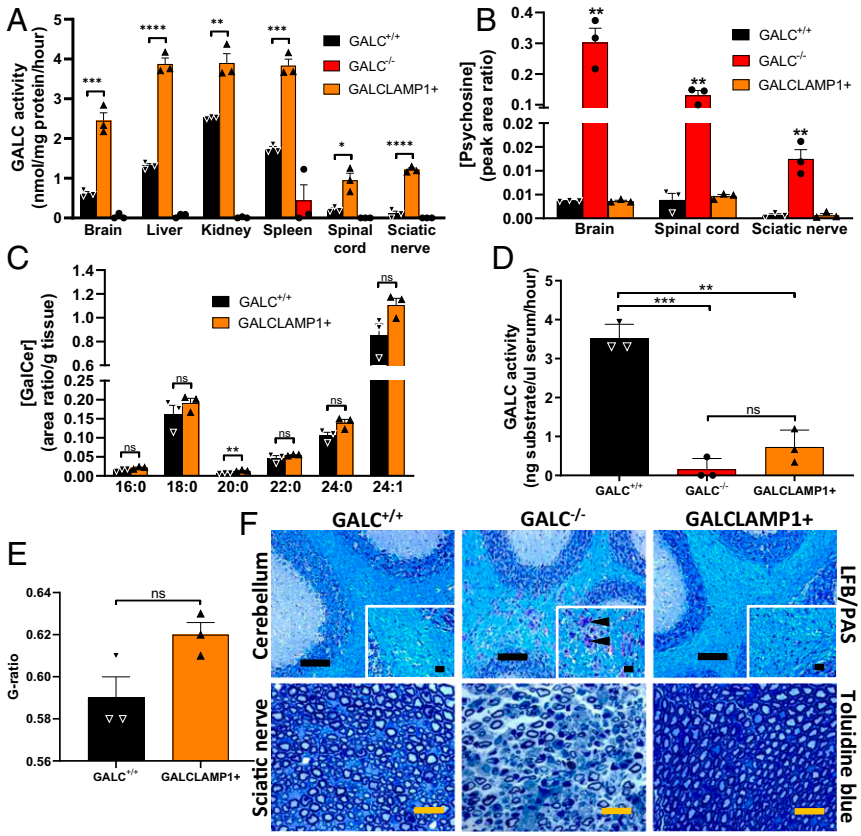

Fig. 2. GALCLAMP1$^+$ mouse biochemistry and histology. (*A*) Mice expressing GALCLAMP1 have high levels of GALC activity in multiple tissues at PND 35 when compared to WT (GALC$^{+/+}$) or Twitcher (GALC$^{-/-}$) animals. (*B*) Psychosine levels at PND 35 are virtually undetectable in both WT and GALCLAMP1$^+$ mice but are significantly elevated in brain, sciatic nerve, and spinal cord of Twitcher mice when compared to either WT or GALCLAMP1$^+$ animals. (*C*) Levels of most galactosylceramide species in GALCLAMP1$^+$ mice are not significantly different from WT at PND 35. (*D*) GALC activity in the serum of GALCLAMP1$^+$ mice is no different from that seen in GALC$^{-/-}$ mice. (*E*) G-ratio of axons is not significantly different at PND 35 between WT and GALCLAMP1$^+$ mice. (*F*) Myelination in the cerebellum of GALCLAMP1$^+$ mice appears similar to WT animals, with no infiltrating globoid cells (*Inset*) and intense myelin staining. Sciatic nerves of GALCLAMP1$^+$ mice contain tightly packed axons with thick myelin, similar to WT animals ($n = 3$ for all groups shown; $^*P < 0.05$, $^{**}P < 0.01$, $^{***}P < 0.001$, $^{****}P < 0.0001$; ns, not significant). (Scale bars: cerebellum, 100 μm; *Insets*, 20 μm; sciatic nerve, 20 μm.)

Although there was no difference in rotarod performance between MPZ^{flox} and GALCLAMP1$^+$ mice, MPZ^{flox} mice have significant motor deficits as measured on the wire hang (Fig. 6*A*). These motor function deficits are delayed when compared to Twitcher mice, with decline beginning at ∼5 wk, and a nadir at ∼16 wk. The animals recover ∼30% of their function at 24 wk but then decline again between 30 and 52 wk. Sciatic nerve pathology and wire hang performance change in tandem up to 16 wk of age (Fig. 6*B*). There is no change in the G-ratio of MPZ^{flox} axons but there is less edema and fewer infiltrating immune cells in the sciatic nerve when compared to Twitcher mice (Fig. 6 *B* and *C*). Pathologic changes become more severe at 16 wk, at which time the sciatic nerves are indistinguishable from Twitcher mice. G-ratio significantly increases in MPZ^{flox} mice when compared to GALCLAMP1$^+$ mice at both 16 and 24 wk (Fig. 6*C*). A significant decrease in nerve conduction velocity (NCV) was seen in MPZ^{flox} mice when tested at 6 and 24 wk (Fig. 6*D* and *SI Appendix*, Fig. S8). A significant decrease in amplitude and increase in latency in both the ankle and sciatic notch of MPZ^{flox} mice is consistent with severe peripheral neuropathy.

Discussion

Although significant alterations (six-glycine linker, LAMP1 transmembrane domain and cytoplasmic tail, and myc tag) were made to GALC in order to prevent its secretion and subsequent cross-correction, the chimeric protein retains enzymatic activity and functions normally both in vitro and in vivo. Maintenance of homeostatic levels of both psychosine and galactosylceramide were two of the most important factors when determining the functionality of membrane-tethered GALC. These data strongly suggest that GALC does not need to be soluble to maintain homeostatic levels of either of its substrates. By all measures analyzed, GALCLAMP1$^+$ animals are indistinguishable from GALC$^{+/+}$, and widespread deletion of GALCLAMP1 fully recapitulates the Twitcher phenotype. Finally, expression of GALCLAMP1 on the normal genetic background (GALC$^{+/+}$) confers no obvious biochemical, histological, or behavioral defects to at least 1 y of age. Taken together, these data validate the utility of this approach to determine the role of specific cells in the pathogenesis of Krabbe disease.

The Schwann cell-knockout mouse (MPZ^{flox}) displays selective motor dysfunction due to the loss of GALC activity in peripheral myelinating cells. On several of the behavioral tests, the MPZ^{flox} mice performed similarly to the GALCLAMP1$^+$ animals. For example, on a motor test that correlates with cerebellar function, the 60-s rotarod, deletion of GALCLAMP1 in myelinating Schwann cells was expected to have little effect on cerebellar pathology or function. This could explain the normal performance of the MPZ^{flox} mice, which have little or no cerebellar pathology, and the poor performance of Twitcher mice, which have profound cerebellar pathology. In contrast, GALCLAMP1 deficiency in Schwann cells has a direct effect on

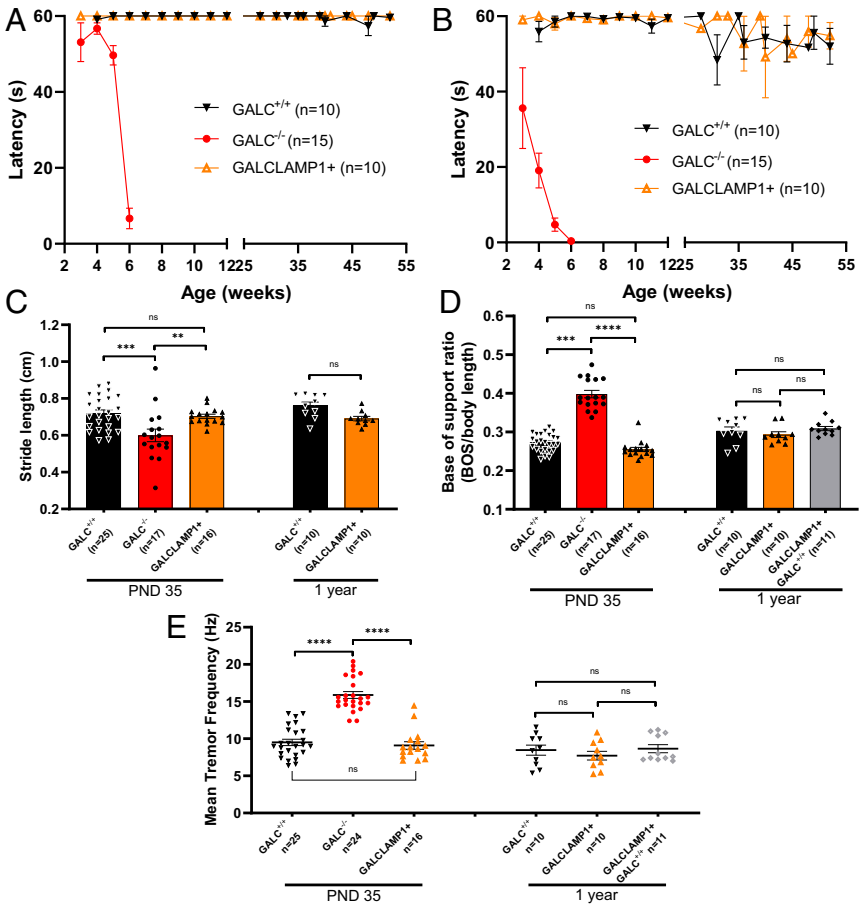

Fig. 3. Behavioral analysis of GALCLAMP1$^+$ animals. (*A* and *B*) When tested on constant-speed rotarod and wire hang, GALCLAMP1$^+$ mice perform at WT (GALC$^{+/+}$) levels through 1 y of age. (*C* and *D*) Stride length and base of support of GALCLAMP1$^+$ mice are not significantly different from WT mice at either PND 35 or 1 y. Expression of GALCLAMP1 in GALC-sufficient mice (GALCLAMP1$^+$ GALC$^{+/+}$) does not alter the base of support at 1 y of age. (*E*) Resting tremor frequency of GALCLAMP1$^+$ mice is not significantly different from WT mice at either PND 35 or 1 y. There is no change in mean tremor frequency in GALCLAMP1$^+$GALC$^{+/+}$ mice (***$P < 0.001$, ****$P < 0.0001$; ns, not significant).

other aspects of the peripheral neuropathy. A significant loss of NCV was observed at 6 and 24 wk in the MPZ^{flox} mice, indicating a profound neuropathy. This is consistent with the decreased number and diameter of axons in the sciatic nerves of MPZ^{flox} mice even though neurons continue to express GALCLAMP1. This is similar to the axonal response in other demyelinating disease models. For example, the *jimpy* and *shiverer* mice (proteolipid protein and myelin basic protein deficiencies, respectively) have severe demyelination/dysmyelination phenotypes (16, 17). This includes significant axonal pathology even though there are no intrinsic neuronal defects in either mouse model. Neither the motor dysfunction measured on the wire hang nor the sciatic nerve pathology progress in a linear fashion as the MPZ^{flox} mice age. Instead, there is a relatively rapid decline in wire hang performance that precedes a transient recovery period, followed by a steady decline out to 1 y. It is unclear why there is a transient improvement in motor function. However, there is an apparent stabilization in axon G-ratio of MPZ^{flox} mice between 16 and 24 wk of age. It has also been previously reported that mature nonmyelinating Schwann cells can redifferentiate into myelinating Schwann cells in response to myelin damage (18). The newly differentiated Schwann cells form thinner myelin sheaths after injury (19). Toluidine blue staining of the sciatic nerves from MPZ^{flox} mice shows thinner myelin sheaths, which is consistent with the redifferentiation of nonmyelinating Schwann cells. Alternatively, it is possible that the more slowly progressing sciatic nerve pathology is due to healthy, GALCLAMP1-expressing macrophages infiltrating the nerve. The infiltration of GALCLAMP1$^+$ macrophages into the sciatic nerve also likely explains the persistence of GALC activity and normalization of psychosine levels with age in the nerve following deletion of the transgene in Schwann cells. Infiltrating GALCLAMP1$^+$ macrophages could also be responsible for clearing debris and improving the functionality of the residual Schwann cells. We see clear evidence of macrophages in the sciatic nerve at 16 wk, and the reduced debris in the interaxonal space could be from their infiltration and clearance of myelin debris. It has been shown previously that GALC-sufficient macrophages are critical to eliminate myelin debris in an induced model of multiple sclerosis (20). However, we believe that it is unlikely that the infiltration of GALCLAMP1-sufficient macrophages alone accounts for the transient improvement in motor function. Rather, we believe that the most likely explanation for the improvement is a combination of remyelination from redifferentiated Schwann cells, the infiltration of GALCLAMP1$^+$ macrophages, and the MPZ^{flox} mice learning to compensate for their motor deficits.

Although Krabbe disease was first described over 100 y ago and the Twitcher mouse has been available for nearly 40 y, we still know very little regarding the role of specific cell types in the progression of the disease. There are many lingering questions about the pathogenesis of Krabbe disease that could be

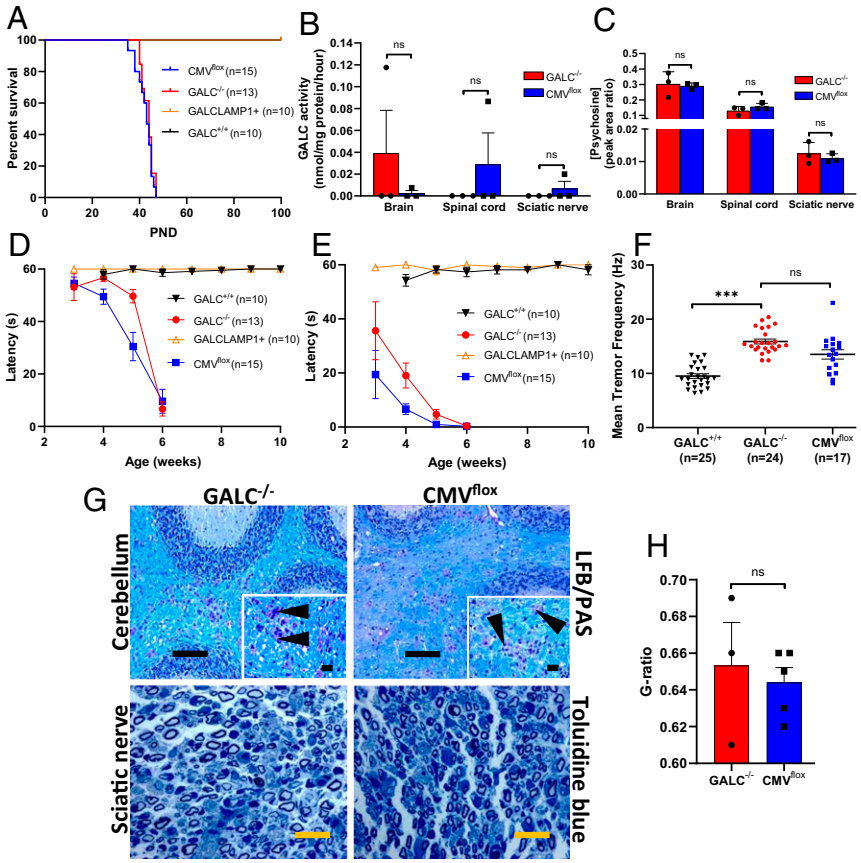

Fig. 4. Characterization of CMV^{flox} animals. (*A*) Lifespan of CMV^{flox} mice is not significantly different from that of Twitcher mice (GALC$^{-/-}$). (*B*) GALC activity is very low in CNS and PNS tissues from PND 35 CMV^{flox} mice, and is not significantly different from Twitcher mice ($n = 3$). (*C*) Psychosine levels in CNS and PNS tissues are elevated in both Twitcher and CMV^{flox} mice ($n = 3$). Psychosine levels are virtually undetectable in WT and GALCLAMP1^{+} animals. (*D* and *E*) When tested on constant-speed rotarod and wire hang, CMV^{flox} mice perform similarly to Twitcher mice. (*F*) Resting tremor frequency of CMV^{flox} mice is not significantly different from Twitcher mice at PND 35. (*G*) Pathology in the cerebellum of CMV^{flox} mice at PND 35 is similar to that in Twitcher mice, with disorganized myelin (blue) and infiltrating globoid cells (*Inset*, arrows) in the white matter tracts. Sciatic nerves of CMV^{flox} mice are similar to Twitcher mice, with large amounts of debris and infiltrating immune cells in the interaxonal space and thinly myelinated axons. (*H*) Axon G-ratio in the sciatic nerve of CMV^{flox} mice is not significantly different from that in Twitcher mice at PND 35 (***$P < 0.001$; ns, not significant). (Scale bars: cerebellum, 100 μm; *Insets*, 20 μm; sciatic nerve, 20 μm.)

elucidated through the implementation of this model. For example, it will be critical to determine the role of oligodendrocytes in the CNS pathology associated with Krabbe disease. In addition, it will be important to determine the role of immune-modulating cells in the progression of Krabbe disease. It is believed that the profound neuroinflammation associated with Krabbe disease accelerates the disease progression. However, it has been shown in at least two different models of LSD that neuroinflammation is actually protective early in the disease process (21, 22). Knocking out GALCLAMP1 specifically in microglia or astrocytes will help resolve this question. Finally, it has been shown that psychosine accumulates in GALC-deficient neurons. Is neuron function directly compromised when GALC activity is not present?

Equally, if not more importantly, this model serves as a proof of concept for expressing soluble lysosomal hydrolases in a cell-autonomous manner. There are at least 50 distinct lysosomal storage disorders, many of which are caused by a deficiency in a soluble acid hydrolase (2). Due to frequent misdiagnosis, the reported frequency of 1:5,000 live births is likely an underestimate (2). Despite the overall prevalence of LSDs, little is known about many of the disorders, and only a small number have an available treatment. Investigating how specific cell types contribute to disease progression is an invaluable route of inquiry that has been nearly impossible to pursue. Although the method described here may not work for all of the lysosomal enzymes, we believe that it could be an effective research strategy for many, if not most, of the lysosomal enzyme deficiencies. Consistent with this hypothesis, lysosomal membrane-tethered forms of two other lysosomal enzymes retained enzymatic activity and prevented the accumulation of their respective substrates (23, 24). However, neither form was inducible. Due to the ubiquitous expression of lysosomal enzymes and broad spectrum of clinical presentations, it is necessary to understand the role of specific cell types when designing effective therapies. Finally, although most lysosomal hydrolases can be secreted from a cell, it is unclear if they have an extracellular function. This model can also be used to more clearly define the role, if any, of secreted lysosomal hydrolases.

Materials and Methods

Chimeric GALCLAMP1, Lentiviral Vectors, and ROSA26-Targeting Vector. The 114-bp transmembrane region and cytosolic tail of LAMP1 (which contains the lysosomal targeting motif; ref. 14) was linked in frame to the C terminus of codon-optimized murine GALC cDNA (a gift from Tal Kafri, University of North Carolina, Chapel Hill, NC) via a six-glycine linker such that GALC is within the lumen of the lysosome. A 30-bp c-Myc epitope tag was linked to the cytoplasmic tail of the LAMP1 domain to complete the GALCLAMP1 transgene. The GALCLAMP1 transgene and the WT codon-optimized GALC cDNA were each cloned into a commercially available lentiviral vector containing the PGK promoter, an SV40 polyadenylation signal, and a puromycin

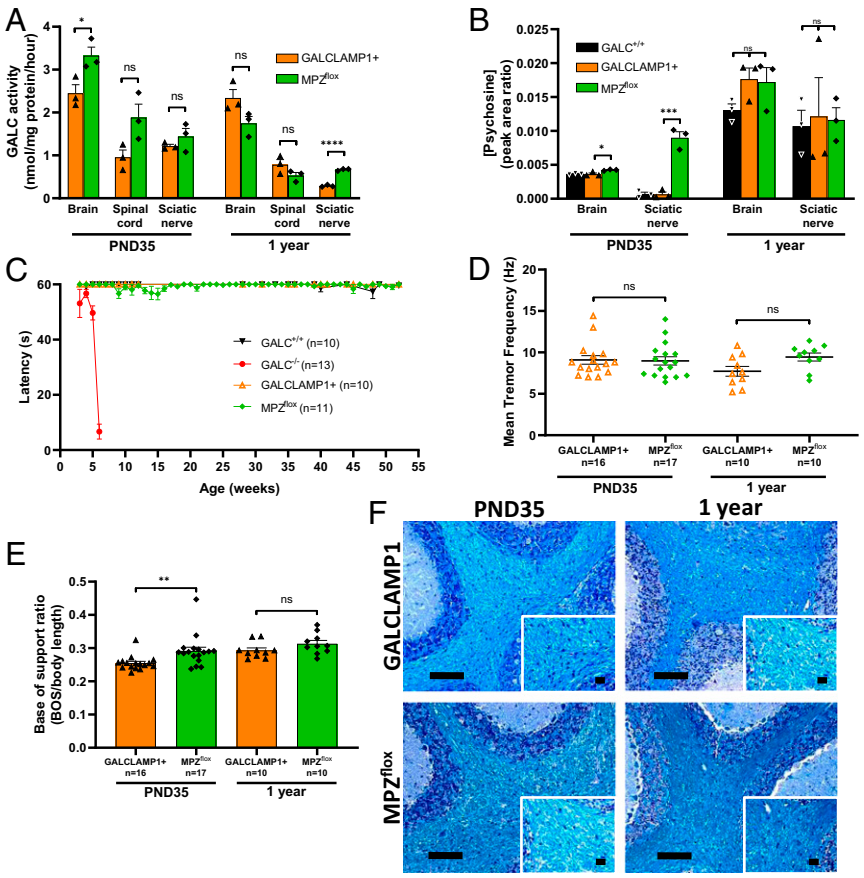

Fig. 5. Characterization of MPZ^{flox} animals. (*A*) There is little difference in GALC activity in the brains, spinal cords, or sciatic nerves between MPZ^{flox} mice compared to GALCLAMP1^{+} mice at PND 35 ($n = 3$ all groups). At 1 y, there is significantly higher GALC activity in the sciatic nerves of MPZ^{flox} mice compared to GALCLAMP1^{+} animals. (*B*) Psychosine is significantly elevated in the sciatic nerves of MPZ^{flox} mice at PND 35 ($n = 3$). No significant increase in psychosine is detected in brain or sciatic nerve at 1 y. (*C*) MPZ^{flox} mice are indistinguishable from GALCLAMP1^{+} mice on rotarod when tested through 1 y of age. (*D*) Resting tremor frequency of MPZ^{flox} mice appears to increase at 1 y but is not significantly different from GALCLAMP1^{+} mice. (*E*) Hind limb base of support is significantly greater in MPZ^{flox} mice when compared to GALCLAMP1^{+} animals at PND 35. There is no significant difference at 1 y. (*F*) Histologically, the cerebellum of MPZ^{flox} mice is similar to that of GALCLAMP1^{+} mice, with intense myelin staining (blue) and no infiltrating immune cells in the white matter tracts at either PND 35 or 1 y (*$P < 0.05$, **$P < 0.01$, ***$P < 0.001$, ****$P < 0.0001$; ns, not significant). (Scale bars: cerebellum, 100 μm; *Insets*, 20 μm.)

resistance cassette (LV-GALCLAMP1, LV-GALC). Infectious lentiviral particles were produced by $CaPO_4$-mediated transient transfection using a four-plasmid system as previously described (25). Unconcentrated viral supernatant was collected 48 and 72 h after transfection and passed through a 0.45-μm filter. The expression cassette for the targeting construct contains the promoter and first intron of the chicken β-actin gene followed by GALCLAMP1 and a rabbit β-globin polyadenylation signal. LoxP sites from a synthetic plasmid were cloned flanking the expression cassette. The conditional expression cassette was then inserted into a targeting vector containing homologous arms that direct insertion into intron 2 of the ROSA locus.

Transduction and GALC Activity Assays. Murine GALC$^{-/-}$ fibroblasts were transduced with either LV-GALCLAMP1 or LV-GALC and selected with 10 μg/mL puromycin added to the media for 1 wk. Cells and media were harvested, and GALC activity was measured using ^{3}H-glactosylceramide (GALC's natural substrate) as previously described (26).

Cell Transfection and Cre-Transduction. Murine GALC$^{-/-}$ fibroblasts were transfected using Turbo DNAfectin 3000 (Lambda Biotech) and the ROSA-targeting GALCLAMP1 expression cassette. Transfection was performed using the manufacturer's instructions. Cells were selected for 2 wk using 10 μg/mL neomycin. After selection, cells were transduced with LV-EF1α-Cre (Addgene, plasmid 11918). Cells were harvested 2 d posttransduction and flash-frozen in liquid nitrogen.

CI-MPR Affinity Chromatography. WT-GALC or GALCLAMP1 were expressed in Expi293 cells after transfection with ExpiFectamine (Life Technologies) using the manufacturer's protocol. After 48 h, the cells were harvested and lysed. CI-MPR assays was performed as previously described (27, 28). Briefly, soluble CI-MPR was purified from FBS and covalently conjugated to Cyanogen bromide-activated Sepharose 4B (Sigma-Aldrich). Aliquots of lysed samples were diluted with buffer A (25 mM Tris-Cl [pH 7.2], 150 mM NaCl, and 1% Triton X-100) and incubated with the CI-MPR beads at 4 °C for 1 h. After incubation, the beads were collected, washed with buffer A, and assayed for GALC activity. Phosphorylation levels are reported as the percentage of the starting enzyme recovered on the beads.

Animal Husbandry and TALEN-Mediated Integration. Twitcher mice on the congenic C57BL/6 background were originally purchased from The Jackson Laboratories (JAX stock no. 000845). Transgenic animals were generated by microinjection of both the ROSA26-targeting vector and ROSA26-specific TALEN mRNA directly into C57BL/6 embryos (JAX stock no. 000664; Transgenic Vectors Core, Washington University). Stable integration of the transgene was confirmed by internal PCR as follows: F1, 5′-ATC AAG GGC TAC TTC GCC TTC GGC ATG CTG-3′; R1, 5′-GCG TGA CTC CTC TTC CTG CCA ATG AGG TAG-3′. Faithful site-specific integration into the ROSA26 locus was confirmed by PCR using primers that crossed the newly created junctions as follows: F2, 5′-CTA AAG AAG AGG CTG TGC TTT GGG GCT CCG-3′; F3, 5′-CGA CTG TGC CTT CTA GTT GCC AGC CAT CTG-3′; R2, 5′-AGA GTG AAG CAG AAC GTG GGG CTC ACC TCG-3′; R3, 5′-CAC TTG TGG TCT TCA GAC ACA CCA GAA GAG-3′. Transgene-positive animals were crossed with GALC$^{+/-}$ mice until GALC$^{-/-}$ homozygosity was achieved. Congenic C57BL/6 and GALC$^{-/-}$ mice were used as controls. CMV^{cre} mice (JAX stock no. 006054) and MPZ^{cre} mice (JAX stock no. 017927) were purchased, and MPZ^{cre} animals were

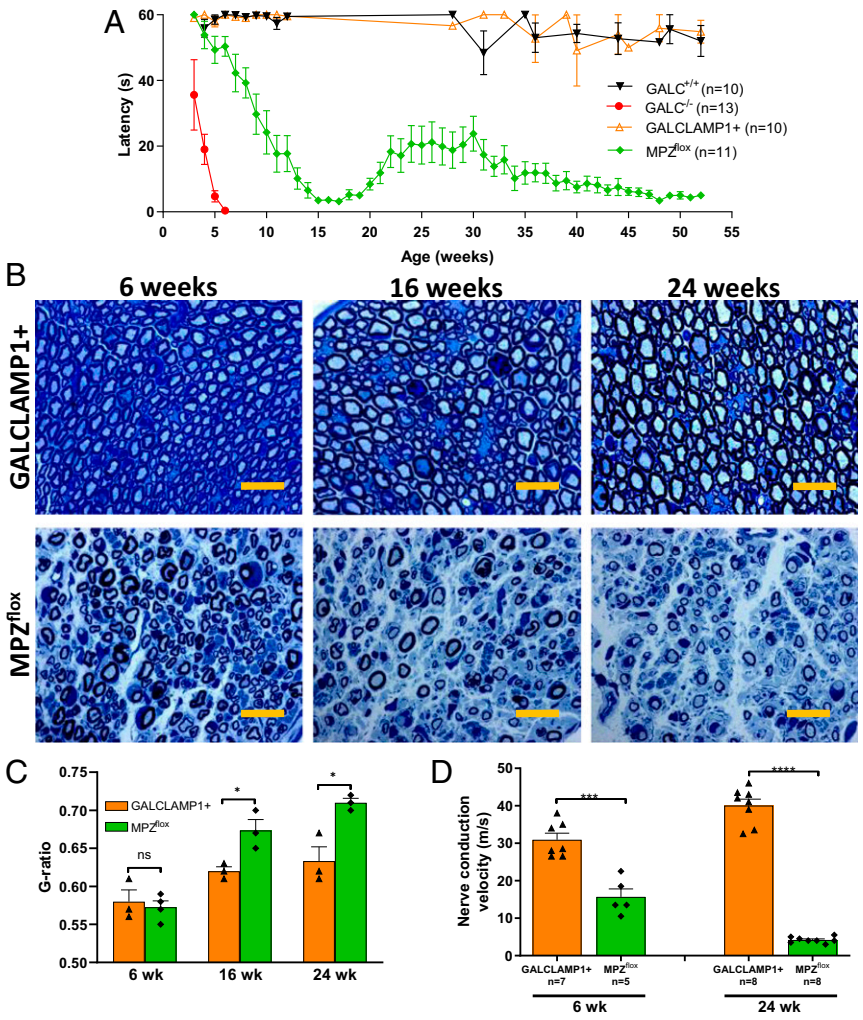

Fig. 6. Peripheral neuropathy of MPZ^{flox} animals. (*A*) A dramatic diphasic decline in wire hang performance is seen in MPZ^{flox} mice when tested out to 1 y. (*B*) Pathology of sciatic nerves correlates with declining wire hang performance. (*C*) Axon G-ratio is no different at 6 wk of age in MPZ^{flox} mice. At both 16 and 24 wk, there is a significant increase in G-ratio when compared to GALCLAMP1^{+} mice. (*D*) Nerve conduction velocity of MPZ^{flox} mice is significantly decreased at both 6 and 24 wk (*$P < 0.05$, **$P < 0.01$, ***$P < 0.001$, ****$P < 0.0001$; ns, not significant).

backcrossed nine generations onto the congenic C57BL/6 background before breeding with the GALCLAMP1 carriers. All mice were maintained by M.S.S. at Washington University School of Medicine and kept on a 12-h light/dark cycle with access to food and water ad libitum. All procedures were carried out in accordance with an approved IACUC protocol (no. 20160213) from Washington University School of Medicine.

Cross-Correction and Cre Responsiveness in Primary Fibroblasts. A primary dermal fibroblast line was isolated and immortalized from a GALCLAMP1$^{+/-}$, GALC$^{-/-}$ animal (GALCLAMP1^{+} cells). After 25 passages, the cells were considered immortalized. GALCLAMP1^{+} cells were transduced with a lentivirus expressing Cre-recombinase (Addgene, plasmid no. 17408) and selected with 10 μg/mL puromycin for 2 wk. After selection, cells exposed to Cre-recombinase (GALCLAMP1^{flox}) and those not exposed to Cre were grown in six-well plates. GALC$^{-/-}$ fibroblasts were plated on transwell inserts (Corning) and incubated separately. After 24 h of growth, the transwell inserts were cocultured with either GALCLAMP1^{flox} or GALCLAMP1^{+} cells for 5 d. All cells were then harvested and frozen in liquid nitrogen for the GALC activity assay.

RNA Extraction and cDNA Analysis. Total RNA was extracted from cell pellets (GALCLAMP1^{+} or LV-GALC) using an RNeasy Mini Kit (Qiagen). RNA integrity number (RIN) was measured with 4200 TapeStation System (Agilent Technologies). The RNA integrity number equivalent (RINe) was determined by the software on the TapeStation System, taking into account the entire electrophoretic trace of the RNA, including the presence or absence of degradation products. Both samples (GALC-myc and GALCLAMP1) exhibited RINe >9.0 and concentrations around 200 ng/uL. Extracted RNA was treated with DNase1 to remove any potential DNA contamination. cDNAs were prepared from the total RNA using the High-Capacity cDNA Reverse Transcription Kit (ThermoFisher Scientific). Presence of codon-optimized GALC cDNA and GALCLAMP1 cDNA was confirmed by PCR using the following primers: GALC F1, 5′-ATC AAG GGC TAC TTC GCC TTC GGC ATG CTG-3′; GALC R1, 5′-GCG GCT TCC ACT CTG AGG TTG TCG AAC TGG-3′; LAMP1 R2, 5′-GCG TGA CTC CTC TTC CTG CCA ATG AGG TAG-3′. Primers recognizing codon-optimized GALC cDNA do not recognize WT GALC transcript.

Psychosine and Galactosylceramide Analysis. GALC-deficient fibroblasts were transduced with LV-GALCLAMP1, and cell division was slowed by reducing the serum to <2%. After 2 wk at near-confluence, cells were harvested and immediately flash-frozen in liquid nitrogen for psychosine analysis. To collect tissues, mice were deeply anesthetized and perfused with phosphate-buffered saline (PBS). Brain, sciatic nerves, and spinal cord were harvested and flash-frozen in liquid nitrogen. Galactosylsphingosine and galactosylceramide were measured as previously described (29). Briefly, tissue samples were homogenized in 0.04 M citric acid. Internal controls in 200 μL methanol were added to 50 μL of each sample. Galactosylsphingosine and galactosylceramide were separated from glucosylsphingosine and glucosylceramide by hydrophilic interaction liquid chromatography (HILIC) columns. Galactosylsphingosine and galactosylceramide were detected using multiple reaction monitoring (MRM) on an AB SCIEX 4000QTRAP tandem mass spectrometer (Atlantic Lab Equipment) using electrospray ionization in

the positive ion mode. Data were processed with Analyst 1.5.2 (Applied Biosystems). Data are reported as the peak area ratios of lipids to their internal standards.

Immunoprecipitation of GALC from Serum. Blood was harvested through cardiac puncture from GALC$^{+/+}$, GALC$^{-/-}$, and GALCLAMP1^{+} animals. Serum was separated through centrifugation, and 25 μL was collected for each assay. Serum was incubated overnight, shaking at 4 °C, with 0.4 μg rabbit anti-GALC antibody (Santa Cruz, sc-293200). Protein A/G PLUS-Agarose Beads (Santa Cruz, sc-2003) were added to serum–antibody mix and incubated for 4 h at 4 °C shaking. Beads were pelleted through centrifugation and rinsed with PBS. Pellets were resuspended in 100 μL H_2O and 100 μL citrate-phosphate buffer (0.1 M citric acid, 0.2 M dibasic sodium phosphate, pH 4.2), and this solution was analyzed in the GALC activity assay as previously described (26). Data are presented as nanograms of substrate cleaved per microliter serum per hour.

Behavioral Analyses. Beginning at week 3 of life, mice were tested weekly for motor deficits using constant-speed rotarod and wire hang until 12 wk of age. After 12 wk, mice were tested monthly unless otherwise noted. Tests were administered as previously described (30). Mice were trained on the rotarod and wire hang at 21 d for three consecutive days. Training consisted of three trials per apparatus, with maximum latency of 60 s on either test. Mice were allowed to rest for 10 min between each training run. On testing days, maximum latency was 60 s on either test, with mice given at least 10 min of rest in between each of three trials. Reported latency is the mean of three trials. Mice were tested on the CatWalk XT (Noldus) and force plate actometer (31) on PNDs 28 and 35 and again at 2, 3, 6 mo, and 1 y of age. A separate cohort of mice were used for the CatWalk and force plate actometer tests due to location of the apparatuses. Mice were habituated to the CatWalk for 15 min on the day prior to first test. On testing day, mice were placed individually in the CatWalk and allowed to freely explore until they performed three qualifying runs, defined as covering a 20-cm stretch with a run speed variation of less than 85%. These exclusion criteria were set due to the high variance in gait of the Twitcher mice. Animals that were unable to meet these criteria were excluded from the study. A custom-made force plate actometer was used to measure resting tremor frequency as previously described (30). Tremor frequency was recorded from transducers at a frequency of 100 samples per second. The most frequently occurring tremor frequency (in hertz) was identified and reported for each mouse following a continuous measuring period of 6 min. An even number of male and female animals were assigned to each behavioral group.

Nerve Electrophysiology. Compound muscle action potentials (CMAPs) were acquired as previously described (32) using a Viking Quest electromyography device (Nicolet). Mice were anesthetized prior to testing, then electrodes were put into place (stimulating ankle or sciatic notch; recording footpad). Supramaximal stimulation was used for CMAPs.

Immunofluorescence in Primary Cells and Brains. Primary fibroblasts from GALCLAMP1^{+} animals were grown on coverslips, and 10 μg/mL wheat germ agglutinin (Thermo Fisher, W11261) was added for 10 min prior to fixing cells to stain the plasma membrane. Cells were fixed in 4% paraformaldehyde for 20 min and permeabilized in 0.01% Triton for 1 h. Primary antibody incubation was overnight at 4 °C, and secondary was 1 h at room temperature. Primary antibodies were rabbit anti-human cMyc (Cell Signaling, no. 2272S; 1:400), mouse monoclonal anti-human cMyc (Santa Cruz, sc-40; 1:200), mouse monoclonal anti-Giantin G1/133 (Enzo, ALX-804–600; 1:2,000), rabbit monoclonal anti-mouse kDel (Abcam, no. 176333; 1:200), rat anti-LAMP1 (PharMingen, 09671D; 1:400; note that the anti-LAMP1 antibody was generated against the luminal domain of LAMP1 so as not to cross-react with the transmembrane and cytoplasmic domains on GALCLAMP1), chicken polyclonal anti-Myelin Protein Zero (Novus Biologicals, NB100-1607; 1:1,500). Secondary antibodies, all from Invitrogen, were Alexa Fluor-conjugated and used at 1:500 dilution: goat anti-rabbit AF488 (A11008), goat anti-mouse AF568 (A11004), goat anti-rat AF488 (A11006), goat anti-mouse AF488 (A11001), and goat anti-rabbit AF568 (A11036).

To collect tissues, mice were deeply anesthetized and transcardially perfused with PBS. Brains were cut sagittally and fixed in 4% paraformaldehyde for 36 h, then transferred into 30% sucrose in Tris-buffered saline (TBS). Brains were mounted in Optimal Cutting Temperature compound (Sakura Finetek) and sectioned at 16 μm using a cryostat. Sections were mounted directly onto Superfrost slides (Fisher Scientific) that had been coated in gelatin-chrome alum. Prior to immunostaining, slides were air-dried for 10 min and rinsed in TBS. Slides were blocked for 1 h in 15% normal goat serum in TBS with 0.01% Triton X-100 (TBS-T). Primary antibody incubation was for 2 h in blocking solution, and secondary was for 2 h. Slides were incubated in 1× TrueBlack (Biotium, no. 23007) for 2 min. TrueBlack was diluted to 1× in 70% EtOH from a 20× stock solution. Slides were rinsed twice in TBS, and coverslips added using DAPI Fluoromount-G (Southern Biotech). Primary antibodies were polyclonal rabbit anti-GFAP (Agilent, no. 20334, 1:1,000) and monoclonal rat anti-mouse CD68 (AbD Serotec/Bio-Rad, MCA1957; 1:400). Secondary antibodies (Invitrogen) were Alexa Fluor-conjugated and used at 1:200 dilution: goat anti-rabbit AF546 (A11010) and goat anti-rat AF488 (A11006).

Histology. Luxol fast blue (LFB) and periodic acid–Schiff (PAS) staining were performed as previously described (30). After anesthesia, mice were transcardially perfused with PBS, and the brain and sciatic nerves were harvested and fixed for 24 h in 4% paraformaldehyde. After fixation in paraformaldehyde for 24 h, brain samples were cryoprotected in 30% sucrose and stored at 4 °C. Tissues were paraffin-embedded for LFB/PAS staining, and 10-μm sections were mounted on slides for staining and analysis. Images were captured using the 20× and 63× (inset) objectives on a Zeiss Axio Imager M2 microscope (Carl Zeiss) using StereoInvestigator software (MBF Bioscience) with all parameters of light intensity, camera setup, and calibration settings kept constant. All images were taken blinded to age and genotype.

Sciatic nerves were immersion-fixed in 2%/4% glutaraldehyde/paraformaldehyde for ≥48 h, incubated in osmium tetroxide, and then serially dehydrated in ethanol. Nerves were then embedded in Araldite 502 (Polysciences), and 1-μm-thick sections were prepared using an ultramicrotome before staining with toluidine blue. Images were captured using the 100× objectives on a Zeiss Axio Imager M2 microscope (Carl Zeiss) using StereoInvestigator software (MBF Bioscience) with all parameters of light intensity, camera setup, and calibration settings kept constant.

Images were analyzed using Image Pro Premier software (Media Cybernetics) by using the Smart Count tool to select axons stained above background levels, with binning used to exclude background by size. Due to the variability in toluidine blue staining from animal to animal, axon diameter and total diameter were measured manually using StereoInvestigator software (MBF Bioscience). At least 30, and up to 60, axons per animal were measured for G-ratio calculations. Data are reported as the mean G-ratio for each animal. All measurements and analyses were performed by someone blinded to age and genotype.

Statistical Analyses. Statistical significance was determined using Student's *t*-test for pairwise comparisons or one-way ANOVA for multiple group comparisons. Due to the unequal variance seen in much of the gait data, stride length and base-of-support measurements were transformed by dividing by each mouse's body length, measured from the nose to the base of the tail. After data transformation, significance was determined by one-way ANOVA with Tukey posttest analysis. All statistical analyses were performed using GraphPad Prism (v8.0).

Data Availability Statement. All data discussed in the paper are either within the manuscript or will be made available to readers via contacting M.S.S. directly.

ACKNOWLEDGMENTS. Codon optimized GALC cDNA was a generous gift from Tal Kafri (University of North Carolina). The ROSA26-targeting vector was a generous gift of Renate Lewis (Washington University). Funding was provided by National Institutes of Health Grants NS100779 to M.S.S. and NS087632 and AG013730 to J.M.

1. A. Ballabio, V. Gieselmann, Lysosomal disorders: From storage to cellular damage. *Biochim. Biophys. Acta* **1793**, 684–696 (2009).
2. M. Fuller, P. J. Meikle, J. J. Hopwood, *Epidemiology of Lysosomal Storage Diseases: An Overview* (Oxford PharmaGenesis, Oxford, 2006), chap. 2.
3. F. M. Platt, B. Boland, A. C. van der Spoel, The cell biology of disease: Lysosomal storage disorders: The cellular impact of lysosomal dysfunction. *J. Cell Biol.* **199**, 723–734 (2012).
4. E. F. Neufeld, J. C. Fratantoni, Inborn errors of mucopolysaccharide metabolism. *Science* **169**, 141–146 (1970).
5. K. Krabbe, A new familial, infantile form of diffuse brain-sclerosis. *Brain* **39**, 74–114 (1916).
6. K. Suzuki, Y. Suzuki, Globoid cell leucodystrophy (Krabbe's disease): Deficiency of galactocerebroside β-galactosidase. *Proc. Natl. Acad. Sci. U.S.A.* **66**, 302–309 (1970).

7. W. C. Lee *et al.*, Suppression of galactosylceramidase (GALC) expression in the twitcher mouse model of globoid cell leukodystrophy (GLD) is caused by nonsense-mediated mRNA decay (NMD). *Neurobiol. Dis.* **23**, 273–280 (2006).
8. N. Baumann, D. Pham-Dinh, Biology of oligodendrocyte and myelin in the mammalian central nervous system. *Physiol. Rev.* **81**, 871–927 (2001).
9. M. Jatana, S. Giri, A. K. Singh, Apoptotic positive cells in Krabbe brain and induction of apoptosis in rat C6 glial cells by psychosine. *Neurosci. Lett.* **330**, 183–187 (2002).
10. E. Haq, S. Giri, I. Singh, A. K. Singh, Molecular mechanism of psychosine-induced cell death in human oligodendrocyte cell line. *J. Neurochem.* **86**, 1428–1440 (2003).
11. L. W. Duchen, E. M. Eicher, J. M. Jacobs, F. Scaravilli, F. Teixeira, Hereditary leucodystrophy in the mouse: The new mutant twitcher. *Brain* **103**, 695–710 (1980).
12. A. B. White *et al.*, Psychosine accumulates in membrane microdomains in the brain of krabbe patients, disrupting the raft architecture. *J. Neurosci.* **29**, 6068–6077 (2009).
13. K. Suzuki, K. Suzuki, The twitcher mouse. A model of human globoid cell leukodystrophy (krabbe's disease). *Am. J. Pathol.* **111**, 394–397 (1983).
14. J. Rohrer, A. Schweizer, D. Russell, S. Kornfeld, The targeting of Lamp1 to lysosomes is dependent on the spacing of its cytoplasmic tail tyrosine sorting motif relative to the membrane. *J. Cell Biol.* **132**, 565–576 (1996).
15. M. L. Feltri *et al.*, P0-Cre transgenic mice for inactivation of adhesion molecules in Schwann cells. *Ann. N. Y. Acad. Sci.* **883**, 116–123 (1999).
16. J. M. Vela, B. González, B. Castellano, Understanding glial abnormalities associated with myelin deficiency in the jimpy mutant mouse. *Brain Res. Brain Res. Rev.* **26**, 29–42 (1998).
17. I. Griffiths *et al.*, Axonal swellings and degeneration in mice lacking the major proteolipid of myelin. *Science* **280**, 1610–1613 (1998).
18. A. Boerboom, V. Dion, A. Chariot, R. Franzen, Molecular mechanisms involved in Schwann cell plasticity. *Front. Mol. Neurosci.* **10**, 38 (2017).
19. J. M. Schröder, Altered ratio between axon diameter and myelin sheath thickness in regenerated nerve fibers. *Brain Res.* **45**, 49–65 (1972).
20. N. J. Scott-Hewitt *et al.*, Heterozygote galactocerebrosidase (GALC) mutants have reduced remyelination and impaired myelin debris clearance following demyelinating injury. *Hum. Mol. Genet.* **26**, 2825–2837 (2017).
21. S. L. Macauley, M. Pekny, M. S. Sands, The role of attenuated astrocyte activation in infantile neuronal ceroid lipofuscinosis. *J. Neurosci.* **31**, 15575–15585 (2011).
22. C. Di Malta, J. D. Fryer, C. Settembre, A. Ballabio, Astrocyte dysfunction triggers neurodegeneration in a lysosomal storage disorder. *Proc. Natl. Acad. Sci. U.S.A.* **109**, E2334–E2342 (2012).
23. S. Marathe *et al.*, Creation of a mouse model for non-neurological (type B) Niemann-Pick disease by stable, low level expression of lysosomal sphingomyelinase in the absence of secretory sphingomyelinase: Relationship between brain intra-lysosomal enzyme activity and central nervous system function. *Hum. Mol. Genet.* **9**, 1967–1976 (2000).
24. C. Shyng, S. L. Macauley, J. T. Dearborn, M. S. Sands, Widespread expression of a membrane-tethered version of the soluble lysosomal enzyme palmitoyl protein thioesterase-1. *JIMD Rep.* **36**, 85–92 (2017).
25. T. Dull *et al.*, A third-generation lentivirus vector with a conditional packaging system. *J. Virol.* **72**, 8463–8471 (1998).
26. D. Lin *et al.*, AAV2/5 vector expressing galactocerebrosidase ameliorates CNS disease in the murine model of globoid-cell leukodystrophy more efficiently than AAV2. *Mol. Ther.* **12**, 422–430 (2005).
27. E. van Meel *et al.*, Multiple domains of GlcNAc-1-phosphotransferase mediate recognition of lysosomal enzymes. *J. Biol. Chem.* **291**, 8295–8307 (2016).
28. L. Liu, W.-S. Lee, B. Doray, S. Kornfeld, Engineering of GlcNAc-1-Phosphotransferase for production of highly phosphorylated lysosomal enzymes for enzyme replacement therapy. *Mol. Ther. Methods Clin. Dev.* **5**, 59–65 (2017).
29. R. Sidhu *et al.*, A HILIC-MS/MS method for simultaneous quantification of the lysosomal disease markers galactosylsphingosine and glucosylsphingosine in mouse serum. *Biomed. Chromatogr.* **32**, e4235 (2018).
30. A. S. Reddy *et al.*, Bone marrow transplantation augments the effect of brain- and spinal-cord-directed AAV 2/5 gene therapy by altering inflammation in the murine model of GLD. *J. Neurosci.* **31**, 9945–9957 (2011).
31. S. C. Fowler *et al.*, A force-plate actometer for quantitating rodent behaviors: Illustrative data on locomotion, rotation, spatial patterning, stereotypies, and tremor. *J. Neurosci. Methods* **107**, 107–124 (2001).
32. B. Beirowski *et al.*, Sir-two-homolog 2 (Sirt2) modulates peripheral myelination through polarity protein Par-3/atypical protein kinase C (aPKC) signaling. *Proc. Natl. Acad. Sci. U.S.A.* **108**, E952–E961 (2011).